

Evolutionary intermittency and the QCD critical point

N. G. Antoniou, F. K. Diakonou, and E. N. Saridakis*

Department of Physics, University of Athens, GR-15771 Athens, Greece

We investigate the dynamics of the critical isoscalar condensate, formed during heavy-ion collisions. Our analysis is based on a simplified model where the sigma and the pions are the only degrees of freedom. In field description, both in physical and momentum space, we find that the freeze-out profile presents a structure which reveals clear traces of the critical fluctuations in the sigma-component. In particle representation, using Monte-Carlo simulations and factorial moment analysis, we show that signatures of the initial criticality survive at the detected pions. We propose the distribution of suitably defined intermittency indices, incorporating dynamical effects due to sigma-pion interaction, as the basic observable for the exploration of critical fluctuations in heavy-ion collision experiments.

I. INTRODUCTION

Experiments of a new generation, with relativistic nuclei, at RHIC and SPS are currently under consideration with the aim to intensify the search for the existence and location of the QCD critical point in the phase diagram of strongly interacting matter [1, 2]. Important developments in lattice QCD [3] and studies of hadronic matter at high temperatures [4] suggest that the QCD critical endpoint is likely to be located within reach at SPS energies. A decisive observation, in these experiments, associated with the development of a second-order phase transition at the critical endpoint of QCD matter is the establishment of power laws in momentum space (self-similarity) in close analogy to the phenomenon of critical opalescence in QED matter [5]. These power laws reflect the fractal geometry in real space, and a characteristic index of the critical behavior is the fractal mass dimension d_{f2} which measures the strength of the order-parameter fluctuations within the universality class of critical QCD [6, 7].

The physics underlying the endpoint singularity in the QCD phase diagram is associated with the phenomenon of chiral phase transition, a fundamental property of strong interactions in the limit of zero quark masses. In this case and for a given chemical potential μ_B there exists a critical temperature T_{cr} above which chiral symmetry is restored and as temperature decreases below T_{cr} ,

*Electronic address: msaridak@phys.uoa.gr

the system enters into the chirally broken phase of observable hadrons. It is believed that, for two flavors and zero quark masses, there is a first-order phase transition line on the (T, μ_B) surface at large μ_B [8]. This line ends at a tricritical point beyond which the phase transitions become of second order. In the case of real QCD with non-zero quark masses, chiral symmetry is broken explicitly and the first-order line ends at a critical point beyond which the second-order transitions are replaced by analytical crossovers [9].

The order parameter of this transition is the chiral field $\Phi = (\sigma, \vec{\pi})$ formed by the scalar, isoscalar field σ together with the pseudoscalar, isovector field $\vec{\pi} = (\pi^+, \pi^0, \pi^-)$. Both fields are massless at the tricritical point and when the symmetry is restored at high temperatures, their expectation value vanishes, $\langle \vec{\pi} \rangle = \langle \sigma \rangle = 0$. However, in the presence of an explicit symmetry breaking mechanism (non-zero quark masses) the pion and sigma fields are disentangled at the level of the order parameter of the QCD critical point, which is now formed by the sigma field alone. The expectation value of the σ -field remains small but not zero near the critical point so that the chiral symmetry is never completely restored. The valuable observables in this case are associated with the fluctuations of the σ -field, $(\delta\sigma)^2 \simeq \langle \sigma^2 \rangle$, and they incorporate, in principle, the singular behavior of baryon-number susceptibility and in particular the power-law behavior of the σ -field correlator [10].

The aim of this work is to study the evolution of critical correlations during the development of a collision of heavy ions ($A + A$), in the neighborhood of the QCD critical point. In the initial state we assume that the system has reached the critical point in thermal equilibrium so that the σ -field fluctuations are described by the 3D Ising critical exponent δ and in particular by the fractal dimension $d_{f2} = \frac{3(\delta-1)}{\delta+1}$ ($\delta \simeq 5$). The crucial question from the observational point of view is whether traces of the initial criticality can survive in the freeze-out regime, which follows the equilibration stage, and leave their imprints at the detectors. In [11] we showed that this is indeed the case for a small class of events. However the treatment presented in [11] has two important disadvantages: (i) the analysis of the fluctuations has been performed in the experimentally inaccessible configuration space and (ii) the determination of the small class of events carrying critical characteristics is by itself a non trivial task. In the present investigation we substantially improve our approach in this direction, achieving at the same time two main goals: (i) better adaptation to experimental requirements, by considering the evolution of the geometry of the critical condensate through intermittency analysis in transverse momentum space and (ii) definition of suitable observables which allow for a quantitative description of the deformation of the critical system by considering all the events in the ensemble. To proceed in this direction we introduce the concept

of evolutionary intermittency in transverse momentum space, which is detectable in heavy-ion collision experiments through factorial moment analysis in an event-by-event basis. Independently from the duration of the freeze-out process, the final profile of the deformed system presents a structure that incorporates all its preceding dynamical history. For its analysis we investigate the distribution of the intermittency indices calculated during the evolution towards the final state. It is shown that this distribution is sensitive to the initial critical state offering a, free from statistical restrictions, tool to explore critical fluctuations.

The dynamics of the system is fixed by a two-field Lagrangian, $\mathcal{L}(\sigma, \vec{\pi})$, together with appropriate initial conditions. The out-of-equilibrium phenomena are generated by the exchange of energy between the σ -field and the environment which consists of massive pions initially in thermal equilibrium. We adopt the picture of a rapid expansion (quench) which is a realistic possibility in this experimental framework. We study the out-of-equilibrium evolution of the σ -field and we impose its decay to pions according to the characteristics of the $\sigma \rightarrow \pi^+\pi^-$ procedure. Since in every collisional event the σ -particles decay independently, time integrations must be taken into account. The freeze-out profile obtained in this way is analyzed both in the field description and particle representation. In order to acquire the particle picture, which is the one obtained in experiments, we use Monte-Carlo simulations of the aforementioned procedure, and the fractal measures are quantified through factorial moment analysis [12, 13].

In section II the formulation of the problem and in particular the equations of motion and the initial conditions are presented. In section III numerical solutions are given in the context of field description in physical and momentum space whereas in section IV we present numerical results in particle framework. Finally, in V our results and conclusions are summarized.

II. THE MODEL

In our approach we assume an initial critical state of the system in thermal equilibrium, disturbed by a two-field potential $V(\sigma, \vec{\pi})$, in an effective description inspired by the chiral theory of strong interactions [14, 15]. The Lagrangian density is

$$\mathcal{L} = \frac{1}{2}(\partial_\mu\sigma\partial^\mu\sigma + \partial_\mu\vec{\pi}\partial^\mu\vec{\pi}) - V(\sigma, \vec{\pi}) \quad (1)$$

with the potential

$$V(\sigma, \vec{\pi}) = \frac{\lambda^2}{4}(\sigma^2 + \vec{\pi}^2 - v_0^2)^2 + \frac{m_\pi^2}{2}\vec{\pi}^2, \quad (2)$$

where $\sigma = \sigma(\vec{x}, t)$ and $\vec{\pi} = \vec{\pi}(\vec{x}, t)$. The potential has the usual σ -model form plus a term which breaks the symmetry along the σ -direction. With the addition of the mass term for the pion field, we ensure that it has a constant mass equal to m_π . Finally, the constant terms in (2) shift the value of the potential at the minimum to zero. We fix the parameters of the Lagrangian using the phenomenological values $m_\pi \approx 139$ MeV, $v_0 \approx 87.4$ MeV and $\lambda^2 \approx 20$ [16].

The equations of motion resulting from (1) are:

$$\begin{aligned} \ddot{\sigma} - \nabla^2 \sigma + \lambda^2(\sigma^2 + \vec{\pi}^2 - v_0^2)\sigma &= v_0 m_\pi^2 \\ \ddot{\vec{\pi}} - \nabla^2 \vec{\pi} + \lambda^2(\sigma^2 + \vec{\pi}^2 - v_0^2)\vec{\pi} + m_\pi^2 \vec{\pi} &= 0, \end{aligned} \quad (3)$$

where $\vec{\pi}^2 = (\pi^+)^2 + (\pi^0)^2 + (\pi^-)^2$.

Using a constant value v_0 in eq. (2) implies a non-vanishing mass (finite correlation length) for the σ -field, $m_\sigma = \sqrt{2\lambda^2 v_0^2}$, in contradiction with its critical profile. This inconsistency is restored if we assume a finite-time mechanism instead of the instant quench i.e. the instantaneous formation of the potential (2) at $t = 0$. The simplest model which leaves the equations of motion unaffected, used also in cosmological phase transitions [17], is the so-called linear quench [11, 18]. It assumes that the minimum v of the potential increases linearly with time, starting from zero and ending at the zero temperature value $v_0 \approx 87.4$ MeV after a time interval τ which is the quench duration:

$$v(t) = \begin{cases} v_0 t / \tau & \text{for } t \leq \tau \\ v_0 & \text{for } t > \tau. \end{cases} \quad (4)$$

This assumption leads naturally to a known evolution of $m_\sigma(t) = \partial^2 V(\sigma, \vec{\pi}) / \partial \sigma^2 |_{\sigma=\sigma_{min}, \vec{\pi}=\vec{\pi}_{min}}$:

$$m_\sigma(t) = \begin{cases} \sqrt{2\lambda^2} \frac{v_0 t}{\tau} & \text{for } t \leq \tau \\ \sqrt{2\lambda^2} v_0 & \text{for } t > \tau. \end{cases} \quad (5)$$

Thus, m_σ presents the expected behavior, i.e. it is $m_\sigma = 0$ at $t = 0$ (critical σ -field) and, with increasing time, m_σ approaches and acquires its zero temperature value $m_{\sigma,0} = \sqrt{2}v_0\lambda$.

We investigate the evolution of the above system using initial field configurations dictated by the onset of the critical behavior. In this case we expect that the σ -field, being the order parameter, will possess critical fluctuations, whereas the π -fields are thermal, and the entire system will be in thermodynamical and chemical equilibrium. Obviously, the subsequent evolution, determined by eqs. (3), will generate strong deviations from equilibrium. The question is whether the initial critical profile (presenting the critical point information) survives for times large enough in order to leave imprints at the freezeout. Before going on with the detailed study of the dynamics, we

first refer to the generation of an ensemble of critical field configurations (initial conditions), and we provide the necessary tools for its quantitative description.

The detailed procedure for the production of the critical ensemble is given in [19]. Interpreting the square of the σ -field as local density, we use the effective action at the critical point [20]:

$$\Gamma[\sigma] = \int_R d^D x \left\{ \frac{1}{2} (\nabla \sigma)^2 + g \sigma^{\delta+1} \right\}, \quad (6)$$

(where δ is the isothermal critical exponent of the corresponding universality class and g is an associated effective coupling) in order to weight the sum over field configurations in the partition function. This sum is saturated through saddle point solutions which consist approximately of piecewise constant configurations extended over domains of variable size [21]. In this way we record a large number of statistically independent configurations possessing critical characteristics, and the corresponding behavior is described by a fractal measure demonstrated in the power-law dependence of the mean "mass" $m_{2x}(R)$ on the distance R around a point \vec{x}_0 defined by:

$$m_{2x}(R) = \int_R |\sigma^2(\vec{x}) \sigma^2(\vec{x}_0)| d^D x d^D x_0 \sim R^{d_{f2x}}, \quad (7)$$

for every \vec{x}_0 . d_{f2x} is the fractal mass dimension of a specific configuration [22, 23], and the subscript 2 marks the use of σ^2 for its definition, while the subscript x indicates the calculation in physical space. d_{f2x} is related to space dimensionality D and isothermal critical exponent δ through:

$$d_{f2x} = \frac{D(\delta - 1)}{\delta + 1}. \quad (8)$$

For the 3D Ising universality class, $g \approx 2$, $D = 3$, $\delta \approx 5$, therefore $d_{f2x|D=3} \approx 2$. The 3D Ising description has to be adapted to the physical framework of colliding nuclei. The considered system may be affected by non-equilibrium processes along the collision axis, and therefore the picture of statistical equilibration is valid safely only for the transverse 2D section. Moreover, the relativistic nature of the longitudinal motion needs an extra assumption (Feynman-Wilson fluid hypothesis [24]) in order to formulate global thermal equilibrium in terms of space-time rapidity. It is then natural to consider the 2D projection of the original 3D Ising system as a description of the fireball in the transverse space. Thus, assuming a cylindrically symmetric fractal, its 2D projection has a mass dimension $d_{f2x|2D \text{ proj}} \equiv d_{f2x} \approx 4/3$, and the σ -field depends only on the transverse coordinates. We produce an ensemble of 10^4 σ -configurations, each one possessing its own fractal mass dimension, and these d_{f2x} 's satisfy (7) and (8) within an error of 2%.

Equivalently, we can define the fractal mass dimension in (transverse) k -space as:

$$m_{2k}(K) = \int_K |\tilde{\sigma}_2(\vec{k}) \tilde{\sigma}_2(\vec{k}_0)| d^2 k d^2 k_0 \sim K^{d_{f2k}}, \quad (9)$$

where $\tilde{\sigma}_2(\vec{k})$ is the 2D Fourier transformation of $\sigma^2(\vec{x})$, and K is the “distance” around a point \vec{k}_0 in the transverse momentum space. Obviously, d_{f2x} and d_{f2k} are related through:

$$d_{f2k} = 2 - d_{f2x}. \quad (10)$$

Performing numerically the aforementioned Fourier transformation, we result in a critical ensemble in k -space satisfying (9), whereas (10) holds within an error of less than 10^{-2} per cent.

Having established the production algorithm for the critical ensemble of the σ -field, and the necessary measures for its quantitative description in physical and k -space, we can proceed to its time evolution. As we have already mentioned in the introduction, we are interested in investigating the evolution of the system determined by equations (3), using as initial conditions an ensemble of 10^4 independent σ -configurations on the lattice possessing critical characteristics, and 10^4 configurations, for each π component, corresponding to an ideal gas at temperature $T_0 \approx 140$ MeV, which simulates the pion environment in a heavy-ion collision. The production of thermal π -configurations has been described in [11, 25].

III. NUMERICAL SOLUTIONS: PHYSICAL AND k -SPACE DESCRIPTION

We evolve the critical system according to (3) and we determine the field values at any time. The quantitative deformation of the initial fractal geometry, is embedded in the evolution of $m_{2x}(R)$ (or of $m_{2k}(K)$ in k -space) and in particular in the evolution of the exponent of its power-law dependence on R . We call this exponent $\psi_x(t)$ (similarly $\psi_k(t)$ in k -space). Initially $\psi_x(0) \equiv d_{f2x}$ (and $\psi_k(0) \equiv d_{f2k}$), i.e. it is the fractal mass dimension of the critical system.

As we showed in [11] $\psi_x(t)$ reaches in short time interval the value of the embedding dimension, which in the present case, due to the projection into transverse space, is equal to 2, and subsequently fluctuates becoming almost equal to $\psi_x(0)$ at particular times. Thus, the initial critical profile reappears partially and quite periodically at times when the spatial mean value of the σ -field returns close to its initial value (which is $\langle\sigma(0)\rangle \approx 0$ as implied by the critical behavior). Finally, after some oscillations $\psi_x(t)$ relaxes very close to 2, i.e. the initial fractal geometry is completely lost. The detailed explanation of this phenomenon is given in [26].

In fig. 1 we depict the evolution of $\psi_x(t)$ and $\psi_k(t)$ for one configuration of the ensemble, using for the quench duration the value $\tau = 5$ fm, where the calculations are achieved through the integrals (7) and (9) at every time. We observe the partial re-establishment of the initial critical profile, and its final complete deformation. Furthermore, we verify that relation (10) holds in very

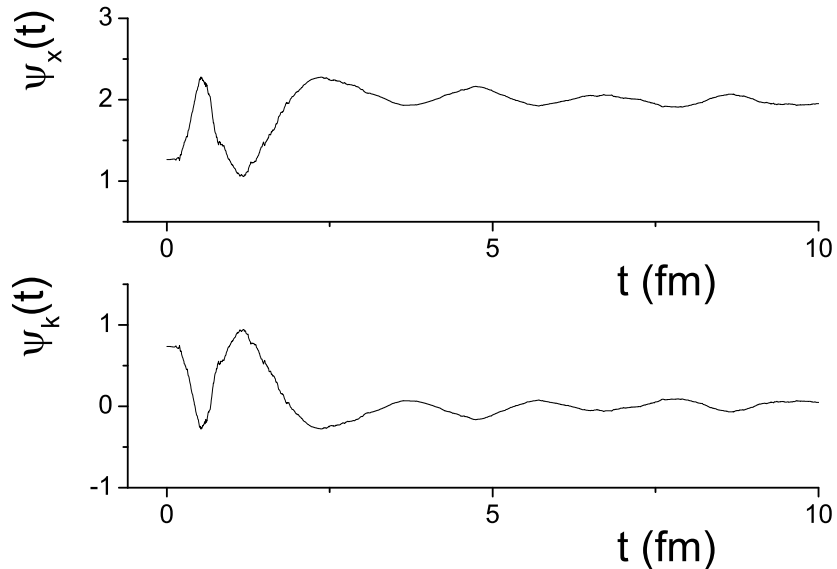


FIG. 1: $\psi_x(t)$ (upper graph) and $\psi_k(t)$ (lower graph) for one configuration, for $\tau = 5$ fm.

good precision at all times. Lastly, a comment must be made for the overflow of $\psi_x(t)$ above the embedding dimension value 2, and equivalently for the negatives values of $\psi_k(t)$. Actually, this result is artificial and it arises from small disturbance, due to finite-size effects, of the linearity of $\ln m_{2x}(R)$ versus $\ln R$, at these time intervals. However, if we proceed to larger lattices, the exceeding of 2 becomes less strong, as we have shown in [26]. This is possible for one event, but it demands extremely huge computational times for the whole ensemble. Therefore, we remain in the aforementioned selection, having in mind that slopes larger than 2 (or less than 0) should be consider as being equal to 2 (or 0). Alternatively, we can avoid this overflow by enforcing a cut on the fit accuracy. As in this work we are interested in the reappearance of the initial fractal geometry, our results are trustworthy being not affected by this behavior.

Now, let us examine the evolution of the whole critical ensemble. To keep the information of the evolution of each individual configuration, i.e. we perform an event-by-event analysis of the ensemble evolution. The reason is that, as we showed in [11], the quantitative characteristics of the initial critical behavior sustaining are more transparent in fluctuation-related measures rather than in ensemble-averaged ones. Thus, at each time instant we calculate a histogram for the distribution $\rho(\psi_x)$, which corresponds to the individual values of $\psi_x(t)$ for each of the 10^4 independent σ -configurations. In fig. 2 we depict $\rho(\psi_x)$ for six successive times. As we can see, initially all the σ -configurations have $\psi_x(0) \equiv d_{f2x}$ equal to the theoretical value $4/3$ (arising from (8) with $D = 2$, $\delta = 5$) within an error of 2%. As time passes, $\psi_x(t)$ for each configuration evolves

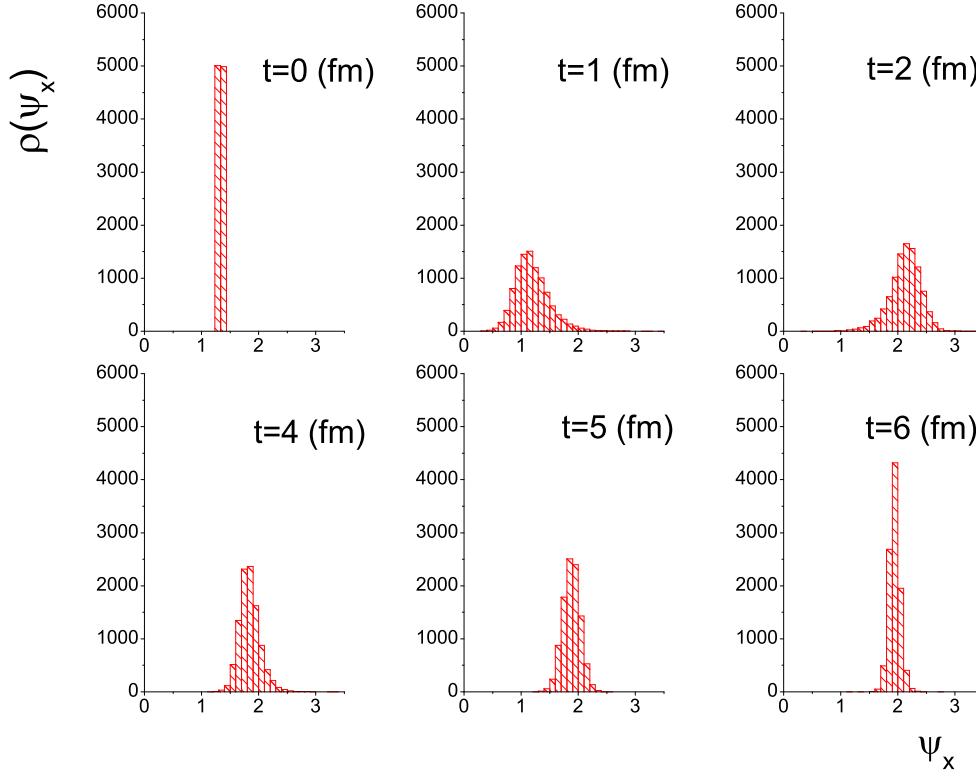


FIG. 2: (color online) Distribution $\rho(\psi_x)$ for the individual values of $\psi_x(t)$ for each of the 10^4 independent σ -configurations, for six successive times, for quench duration $\tau = 5$ fm.

independently (similarly to fig. 1) and both the maximum and the standard deviation of $\rho(\psi_x)$ changes. However, as we can clearly observe, the non-trivial fractal geometry prevails for some time in a subset of the ensemble, and eventually disappears leading to $\rho(\psi_x)$ centered at the value of the embedding dimension 2, with decreasing standard deviation, i.e. all configurations do gradually lose their initial critical profile. Similarly, we repeat the same steps for the k -space-defined $\psi_k(t)$, and the corresponding evolution of $\rho(\psi_k)$ is depicted in fig. 3. The explanation of the behavior of $\rho(\psi_k)$ is straightforward, and as expected the loss of the initial critical behavior is reflected to an increasingly narrower distribution $\rho(\psi_k)$ centered at zero.

The above evolution of independent configurations is unrealistic and is only useful in order to demonstrate the fractal geometry reappearance. In fact, after $m_\sigma(t)$ reaches the threshold of $2m_\pi$ at time t_{th} which according to (5) is:

$$t_{th} = \frac{2m_\pi\tau}{\sqrt{2\lambda^2v_0}}, \quad (11)$$

the σ -particles can decay to pions through $\sigma \rightarrow \pi^+\pi^-$. Thus, traces of the initial criticality can be transferred to the produced pions. In [11] we were interested mainly in the qualitative description

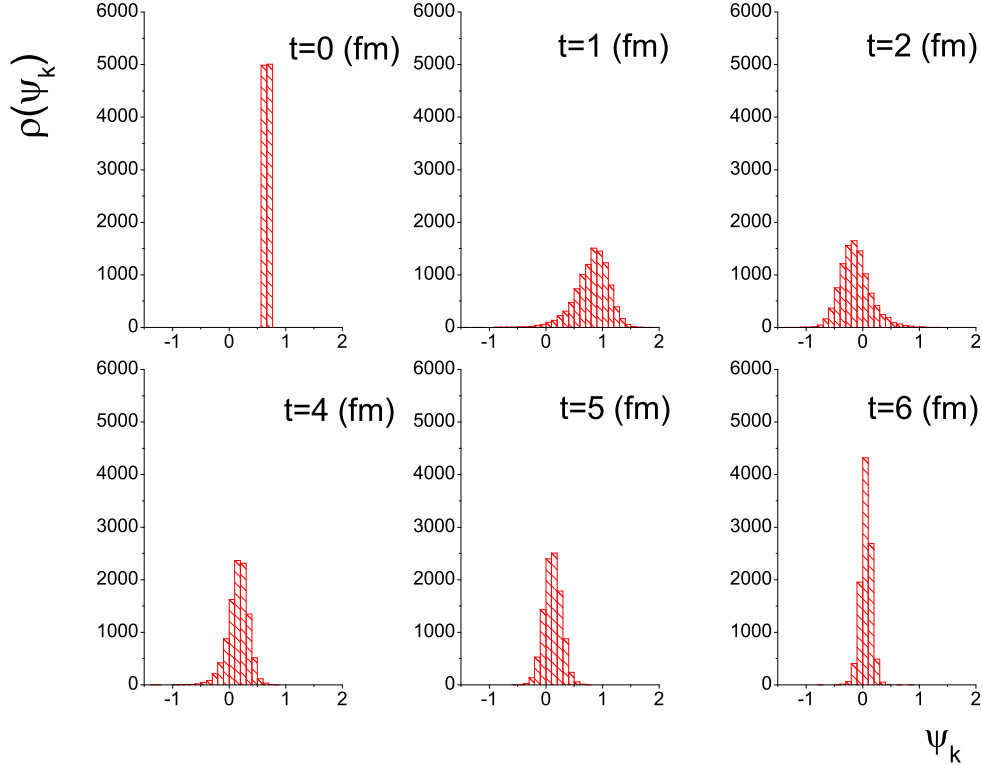


FIG. 3: (color online) Distribution $\rho(\psi_k)$ for the individual values of $\psi_k(t)$ for each of the 10^4 independent σ -configurations, for six successive times, for quench duration $\tau = 5$ fm.

of this phenomenon and we showed that signs of the initial critical behavior can indeed be found in the pion sector. In the present work we proceed to a detailed and more quantitative analysis. To achieve this, we first have to specify the width of the σ -decay. This is given by the expression: $\Gamma(t) = \Gamma_0 \sqrt{1 - (2m_\pi/m_\sigma(t))^2}$, which is easily treated in our approach since we have assumed a specific (and quite general) form for the quench evolution and consequently for $m_\sigma(t)$ (relation (5)). Therefore, for the decay width we acquire:

$$\Gamma(t) = \begin{cases} 0 & \text{for } t < t_{th} \\ \Gamma_0 \sqrt{1 - \frac{4m_\pi^2}{2\lambda^2 v_0^2} \frac{\tau^2}{t^2}} & \text{for } t_{th} \leq t \leq \tau \\ \Gamma_0 \sqrt{1 - \frac{4m_\pi^2}{2\lambda^2 v_0^2}} & \text{for } \tau < t. \end{cases} \quad (12)$$

The factor Γ_0 can be determined by fixing the value of the σ -width at zero temperature. Eq. (12) allows us to determine the probability density $\rho_{dec}(t)$ that a σ -particle will decay at t , using the definition of $\Gamma(t)$ in the particle picture: $\frac{dN_\sigma}{dt} = -\Gamma(t)N_\sigma$ and neglecting any influence of the surrounding thermal medium, as well as regeneration effects. The probability $P(t)$ to decay a sigma particle in the time interval $[0, t)$, assuming that each sigma decays statistically independent

from the others, is then given as:

$$P(t) = \frac{N_\sigma(0) - N_\sigma(t)}{N_\sigma(0)} = 1 - e^{-\int_0^t \Gamma(z) dz}$$

leading to:

$$\rho_{dec}(t) = \frac{dP}{dt} = \Gamma(t)e^{-\int_0^t \Gamma(z) dz}$$

We finally get the expression:

$$\rho_{dec}(t) = \begin{cases} 0 & \text{for } t < t_{th} \\ \Gamma_0 \sqrt{1 - \frac{4m_\pi^2 \tau^2}{m_{\sigma,0}^2 t^2}} e^{-\Gamma_0 \left[\sqrt{t^2 - \frac{4m_\pi^2}{m_{\sigma,0}^2} \tau^2} - \frac{2m_\pi}{m_{\sigma,0}} \tau \arccos\left(\frac{2m_\pi \tau}{m_{\sigma,0} t}\right) \right]} & \text{for } t_{th} \leq t \leq \tau \\ \Gamma_0 \sqrt{1 - \frac{4m_\pi^2}{m_{\sigma,0}^2}} e^{-\Gamma_0 t \sqrt{1 - \frac{4m_\pi^2}{m_{\sigma,0}^2}} + \frac{2m_\pi}{m_{\sigma,0}} \Gamma_0 \tau \arccos\left(\frac{2m_\pi}{m_{\sigma,0}}\right)} & \text{for } \tau < t. \end{cases} \quad (13)$$

Equation (13) leads to a distribution for the mass of the decaying σ 's with a characteristic peak at m_σ^* , which for $\tau \rightarrow \infty$ tends to the threshold value $2m_\pi$ ($m_\sigma^* |_{\tau \rightarrow \infty} \rightarrow 2m_\pi$). Qualitatively, this behavior corresponds to the singular enhancement of the spectral density of the sigma field in medium ($\rho_\sigma(\omega) \sim \left[1 - \frac{4m_\pi^2}{\omega^2}\right]^{-1/2}$) in the case of partial symmetry restoration [27]. In practice, using $\tau = 5 fm$ we get $m_\sigma^* \approx 282 MeV$ (leading to a decay width $\approx 130 MeV$) which is very close to the two-pion threshold, and the associated σ -mass distribution resembles, within our simplified approach, the in-medium spectral properties of the sigma field at the critical point. In the upper graph of fig. 4 we depict $\Gamma(t)$ for $\tau = 5 fm$, taking $\Gamma_0 = 800 MeV$ and $m_{\sigma,0} \approx 560 MeV$, while in the lower graph we show the corresponding $\rho_{dec}(t)$.

Having formulated the quantitative treatment of σ -decay we can proceed to our investigation. The scenario we explore is the following: We evolve the ensemble of 10^4 critical σ -configurations in an environment of thermal pions. After t_{th} each one of them will decay independently according to $\rho_{dec}(t)$ given by (13), i.e. each configuration will decay at each own t_{dec} , and this corresponds to a single event. However, experimentally we get only a freeze-out profile of events, since there is no available information concerning the decay time at which the pions, observed at the detectors, were produced. To acquire this profile we have to dress the evolution of $\rho(\psi_x)$ with the decay probability $\rho_{dec}(t)$. Therefore, the event-by-event freeze-out profile in physical space will be the integral of $\rho_{\psi_x}(t)$ weighted with $\rho_{dec}(t)$, up to a final time corresponding to the freeze-out time t_{frz} :

$$\rho_{w\psi_x}(t_{frz}) = \int_0^{t_{frz}} \rho_{\psi_x}(t) \rho_{dec}(t) dt. \quad (14)$$

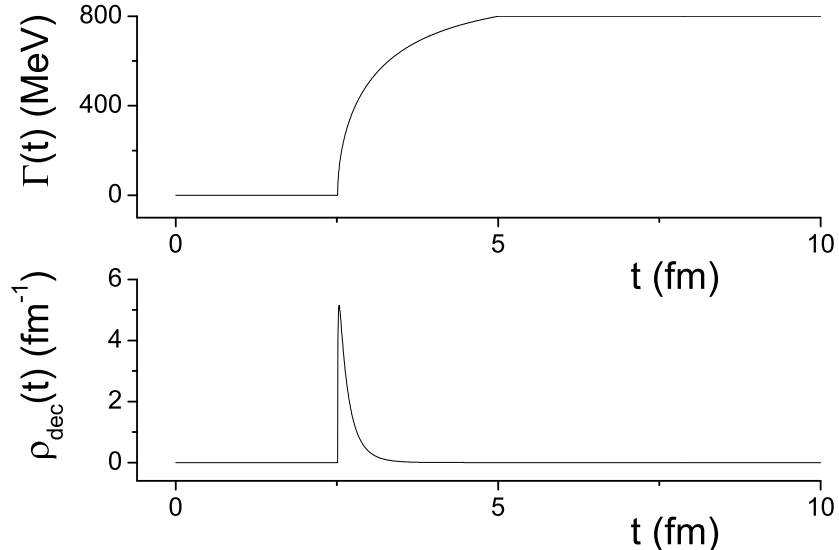


FIG. 4: Decay width $\Gamma(t)$ and $\rho_{dec}(t)$ for $\tau = 5$ fm, $\Gamma_0 = 800$ MeV and $m_{\sigma,0} \approx 560$ MeV.

Although in general the weighted integral has to be performed up to infinite freeze-out time, (or up to its experimentally determined value), due to the exponential decrease of $\rho_{dec}(t)$ all the profiles with freeze-out times t_{frz} larger than $t_* \approx 10$ fm are practically identical. Similarly, the corresponding profile in k -space will be the weighted integral $\rho_{w\psi_k}(t_{frz})$ of $\rho_{\psi_k}(t)$ with $\rho_{dec}(t)$.

In fig. 5 we depict this freeze-out profile, both in physical and k -space, for freeze-out time $t_{frz} = 10$ fm (normalized to give the correct event-multiplicity, i.e. 10^4). As we observe, apart from the main peak at 2 in physical space (the main peak at 0 in k -space) which corresponds to complete loss of the initial critical behavior, there is a secondary “shoulder” which is a result of the time history of all the events that preserved traces of their initial critical profile at their decay-time t_{dec} . This secondary structure is a safe and robust signature of the initial criticality. Furthermore, it is also univocal, since starting from conventional (non-critical) initial conditions it is impossible to acquire even one non-conventional event at freeze-out, as we have shown in [11].

IV. NUMERICAL SOLUTIONS: MONTE-CARLO SIMULATION

In the previous section we investigated the evolution of the critical system, constituted by a large number of individual events, based on the elaboration of the σ and $\vec{\pi}$ fields. In this section we proceed to a more advanced description and refer to particles, since these are the entities that are detectable. This process demands a sequence of steps in order to bring our treatment closer to

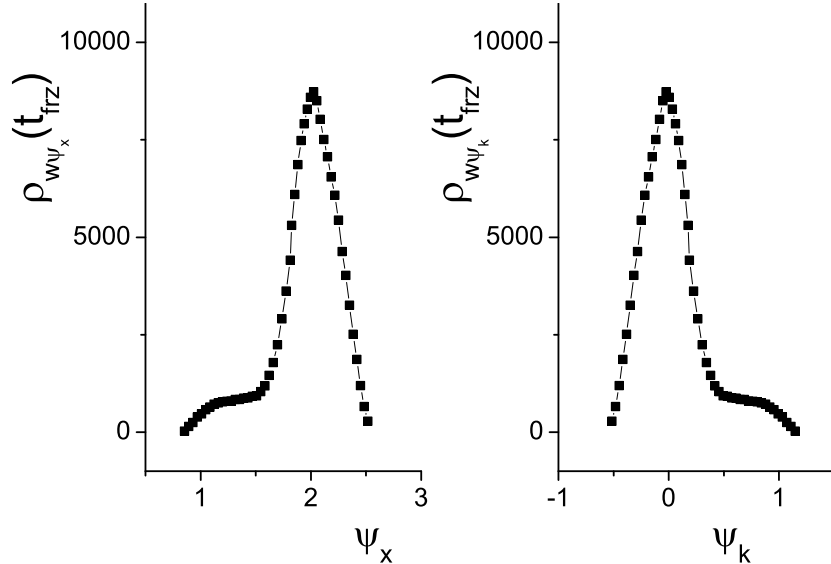


FIG. 5: On the left the freeze-out profile in physical space, given as the weighted integral $\rho_{w\psi_x}(t_{frz})$ of $\rho_{\psi_x}(t)$ with $\rho_{dec}(t)$, for $t_{frz} = 10$ fm. On the right the corresponding profile in k -space, given as the weighted integral $\rho_{w\psi_k}(t_{frz})$ of $\rho_{\psi_k}(t)$ with $\rho_{dec}(t)$, for the same freeze-out time.

the conditions present in a heavy-ion collision experiment.

In our study we use σ -configurations which correspond to single events and we assign to each of them a σ -multiplicity of ≈ 140 σ 's. This corresponds to $A + A$ collisions with intermediate size nuclei assuming the ideal case when the charged pions observed in the (hypothetical) detector originate exclusively from the decay of these sigmas and they do not suffer final state interactions. In fact, the integral: $\int_V \sigma^2(\vec{x})d\vec{x}$ is much larger than the integral: $\int_V \pi^2(\vec{x})d\vec{x}$ for all times. Therefore, interpreting σ^2 as the sigma-particle density and π^2 as the pion density, the above property indicates that at criticality the multiplicity of the pions in the thermal environment is much smaller than the corresponding σ -multiplicity. Now, the presence of a large number of sigma-particles per event can dramatically complicate things since every σ -particle within an event can decay independently, and there is no consistent formalism for treating the subsequent evolution of the σ -field after its partial decay. However, since $\rho_{dec}(t)$ has a sharp peak, we assume that all the σ 's within a single event decay at the same t_{dec} , which is of course varying for the different events of the ensemble.

Conclusively we follow this procedure: We evolve each configuration (individual event) according to (3). We determine the corresponding t_{dec} according to $\rho_{dec}(t)$, and at this specific time we find the 2D Fourier transformation $\tilde{\sigma}_2(\vec{k})$ of the square of the σ -field $\sigma^2(\vec{x})$. Then we produce the momentum components of each of the 140 particles through a Monte-Carlo simulation of this

momentum profile. Knowing the momenta of the σ -particles we can easily use the kinematics of the decay $\sigma \rightarrow \pi^+\pi^-$, in order to determine the momenta of the produced pions, similarly to the previous work [7]. Note that our algorithm allows a loss of information through the secondary decay $\sigma \rightarrow 2\pi^0$, and therefore the produced pion pairs are less than the 140 σ 's (they vary between 80 and 100, i.e. around the two thirds of the σ -multiplicity). Finally, we repeat this procedure for the whole ensemble of events.

In particle representation, the requisite statistical tool for the quantitative description of the fractal properties is the factorial moment analysis. We first perform a partition of the two-dimensional transverse k -space into M^2 cells, and we calculate the particle multiplicity n_m inside each cell. Then we repeat this for all possible cell sizes (between two scales). The corresponding second factorial moment is defined as:

$$F_2(M) = \frac{\frac{1}{M^2} \sum_{m=1}^{M^2} n_m(n_m - 1)}{\left(\frac{1}{M^2} \sum_{m=1}^{M^2} n_m\right)^2}, \quad (15)$$

and for a critical profile, corresponding to isothermal critical exponent δ , this two-dimensional transverse moment analysis leads to the power law:

$$F_2(M) \sim (M^2)^{f_2}, \quad (16)$$

with the exponent f_2 given by:

$$f_2 = \frac{\delta - 1}{\delta + 1}. \quad (17)$$

f_2 is called ‘‘intermittency index’’, since (16) determines the self-similarity of the multi-particle state spectrum, when it is being analyzed in different scales, the so-called intermittency [7, 12, 13]. Note that since we work in the framework of event-by-event analysis throughout this study, we define the second factorial moment for each of the individual configurations, and thus we do not perform event averaging in (15) which is usually taken in the literature. This leads to a slight decrease in the quality of the fit in $F_2(M)$ vs M^2 graph, due to reduced statistics. However, as we have already mentioned, the event-by-event analysis reveals rich information about the fluctuations evolution, which remains hidden in an average analysis.

There is one last problem that remains to be solved, before the framework of our approach is completed. Although, given the σ -particle momenta, we can verify relation (16) in large accuracy, the pion analysis presents a complication. In an event of a heavy-ion collision the majority of the σ -particles decays to a pair of π^+, π^- , while the rest decay to neutral pions which cannot be detected straightforward. However, in the detectors we record all the charged pions of an

event simultaneously, and thus we cannot find which pairs of them come from the same σ , in order to reconstruct them and compute the factorial moments correctly. A more sophisticated reconstruction procedure is necessary, and it has been elaborated in [6]. The basic features are the following: We first choose a narrow invariant mass window, located just above the two-pion threshold, to perform the reconstruction of the sigma field. This is dictated by the form of the m_σ -distribution (which for $\tau = 5 fm$ is peaked at $m_\sigma^* \approx 282$ MeV) and is compatible with the spectral properties of the critical sigma-field in medium due to the partial restoration of chiral symmetry [27]. We then combine all π^+ with all π^- within a single event making di-pions, and we record the subset of them that has invariant mass inside the selected window. Obviously, some of these di-pions correspond to real σ 's, but some of them (usually the majority) consist a combinatorial background modifying the value of the factorial moments. This background can be simulated by di-pions reconstructed from mixed events and it is removed by the subtraction of the corresponding moments. The corrected factorial moments reveal, to a large extent, the behavior of the σ 's before their decay. Moreover, this subtraction eliminates also the thermal pions that are present in our model and give conventional contribution to the factorial moments. We point here that in the reconstruction procedure there is an additional information loss, concerning the initial sigma state, in the neutral pion channel. Furthermore, performing it event by event it stiffens the procedure due to the low statistics. However, in the end we re-acquire an exponent of the factorial moments that is equal to the expected within an error of less than 5%.

Having formulated our method, we can proceed to numerical simulation, verifying first the validity of our approach at each step. In order to test the Monte-Carlo procedure and the factorial moment analysis in the σ -sector, we simulate the decay of the initial critical σ -configurations (corresponding to $\delta = 5$) and we perform moment analysis on the produced σ -particles. In subfigure 6a we depict the second factorial moment for each one of the events and in subfigure 6b we present the corresponding R^2 values which control the quality of the linear fit. R^2 is defined as:

$$R^2 = \frac{(\langle y\tilde{y} \rangle - \langle y \rangle \langle \tilde{y} \rangle)^2}{(\langle y^2 \rangle - \langle y \rangle^2)(\langle \tilde{y}^2 \rangle - \langle \tilde{y} \rangle^2)},$$

where y are the values for a given measure Y while \tilde{y} are the corresponding values of the fitting function. Each value of these histograms arise from a single event, where the corresponding second factorial moment plot is like the one shown in subfigure 6c (here we show an event with slope that is one fifth standard deviations from the histogram average). As we can see from the $\rho(f_2)$ histogram, the obtained f_2 values in the σ -particle sector are distributed around the theoretical expectation $f_2 = 2/3$ according to relation (17). The width of the distribution in general depends

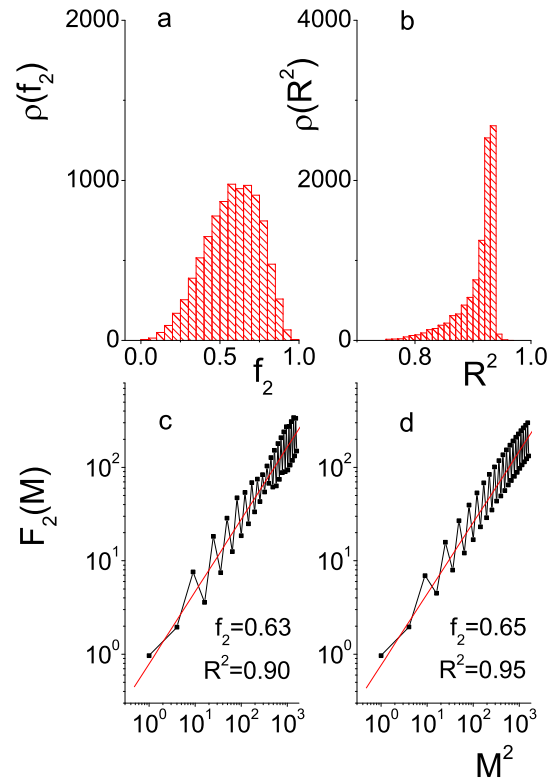


FIG. 6: (color online) In graph a) we present the histogram $\rho(f_2)$ of the exponents f_2 of the second factorial moment for each one of the events, in the case of σ -particles produced directly from the critical ensemble corresponding to $\delta = 5$. In graph b) we show the corresponding values of R^2 which determine the precision of the fits. In graph c) we depict the second factorial moment of a single event (with slope less than one fifth standard deviations away from the histogram average). In graph d) we present the average second factorial moment, which is usually used in the literature.

on the multiplicity of σ -particles per event which in our case is fixed to 140. Thus, within our treatment the critical profile of the σ -particles, through both Monte-Carlo simulation and factorial moment analysis, is reproduced in a consistent way. Lastly, in fig. 6d we depict the usually calculated average second factorial moment. Although linearity (described by R^2) is here better and the obtained slope is close to the expected one, the average calculation has the disadvantage of information loss due to the replacement of the entire structure of the $\rho(f_2)$ -histogram by a single value. As we see in the following the overall structure of the intermittency index histogram proves to be very important and this is the reason why we insist on the event-by-event analysis. Finally, note here that the average factorial moment of fig. 6d is not exactly the average of the histogram

$\rho(f_2)$, since in the former case the mean is calculated before the sum in relation (15), while in the latter we take the average of the slopes.

Having verified our approach at the level of the initial σ -configuration we can proceed to the time evolution. We evolve the system of 10^4 critical σ -configurations (events) in an environment of 10^4 thermal pion-configurations and we let them decay independently according to $\rho_{dec}(t)$. From each configuration we get 140 σ -particle momenta through Monte-Carlo simulation, and using kinematics we perform the decay with a branching ratio 2:3 to π^+, π^- pairs. These are simultaneously detected at the freeze-out (similarly to the previous section we use a value of $t_{frz} = 10$ fm which is by far satisfactory), prohibiting the identification of the original σ 's. Thus, as stated above, due to the combinatorial background, a simple factorial moment analysis will not be sufficient to reveal the critical properties of the decaying system. Indeed, in fig. 7 we present the corresponding four graphs of the moment analysis at the freeze-out. In subfigure 7a we show the histogram $\rho(\zeta)$ of the exponent ζ for the charged pions, which for a fractal profile is equal to $f_2 = 2/3$ according to (17), and in subfig. 7b we give the corresponding R^2 values. In subfig. 7c we depict the second factorial moment for a single event (with slope less than one third standard deviations away from the histogram average) while in 7d we present the average factorial moment for the whole ensemble of events. As we mentioned, the simultaneous detection of all the pions suppresses in this sector the signal associated with the partial restoration of the critical sigma profile, and reduces the obtained ζ 's values. Thus, in order to recover the signature of the initial fractal geometry, the previously described more sophisticated reconstruction procedure is necessary.

In fig. 8 we depict the results of the factorial moment analysis for the pions at the freeze-out, after the reconstruction step, using an analysis window of 10 MeV just above the two-pion threshold $2m_\pi$. This particular choice is appropriate since it includes the $m_{\pi^+\pi^-}$ invariant mass value which corresponds to the maximum of the mass distribution of the decaying sigmas ($m_\sigma^* \approx 282$ MeV). In addition, in this kinematical window the probabilities of the appearance of $(\pi^+\pi^-)$ -pairs originating from the decay of conventional resonances (as for example the ρ -meson) is vanishingly small. Furthermore, performing our analysis so close to the two-pion threshold has another advantage: at these invariant-mass values the re-generation of sigmas from the pions will be small, i.e the generation of a σ -particle with this constrained invariant-mass, from pions produced by primary sigma decay, is statistically rare, which provides a justification for non-consideration of re-generation effects. Finally, the mean multiplicity of σ 's, before reconstruction, within this window is ≈ 60 . $\Delta F_2(M)$ stands for the corrected factorial moments, which arise after the subtraction of the moments of the mixed events. The reconstruction procedure in the event-by-event analy-

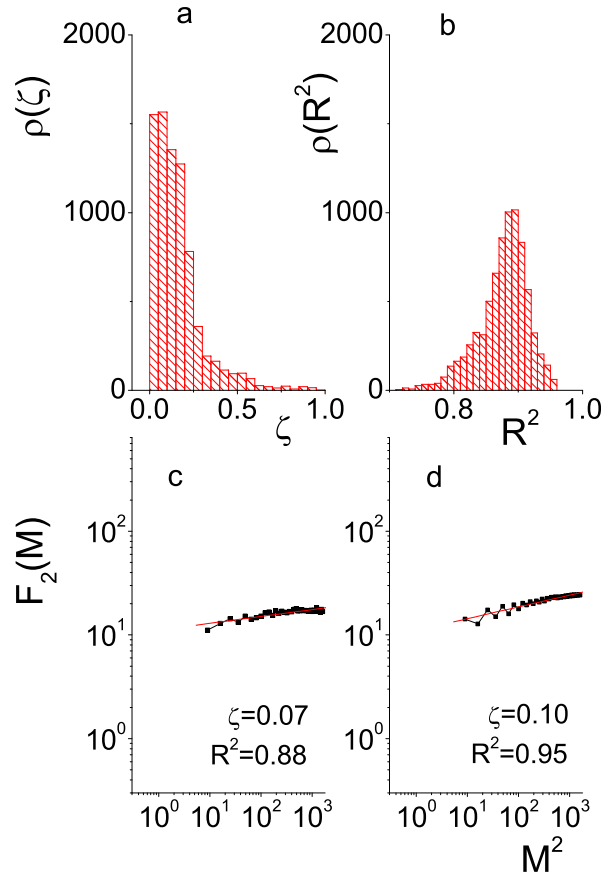


FIG. 7: (color online) In graph a) we present the histogram $\rho(\zeta)$ of the exponents ζ of second factorial moment, for all the event population, arising from a conventional moment analysis, in $\delta = 5$ case, for $t_{f_{rz}} = 10$ fm. In graph b) we show the corresponding values of R^2 which determine the precision of the fits. In graph c) we depict the second factorial moment of a single event (with slope less than one third standard deviations away from the histogram average), for $t_{f_{rz}} = 10$ fm. In graph d) we present the average second factorial moment, for $t_{f_{rz}} = 10$ fm.

sis, compared to the reconstruction in the whole ensemble which is widely used in the literature, possesses some additional problems. Firstly, in a small fraction of events the subtraction of the moments of the mixed pions leads to negative moments. This is a sign that for these events, and at the specific cell partition, the reconstruction procedure did not work and therefore they have to be excluded. Secondly, another fraction of reconstructed events possesses positive moment values with slopes (i.e. ζ -values) smaller than 0 or greater than 1. This is also a result of an unsuccessful reconstruction and means that their profile is completely overwhelmed by the background of mixed events. Both these problem sources have their origin in the low statistics of the event-by-event

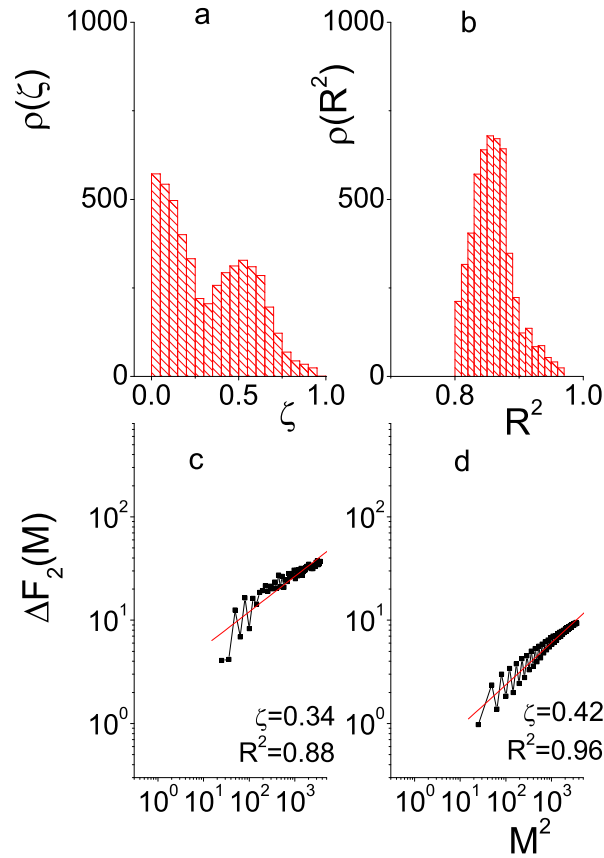


FIG. 8: (color online) In graph a) we present the histogram $\rho(\zeta)$ of the exponents ζ of second factorial moment, for all the event population at the freeze-out ($t_{frz} = 10$ fm), performed after the reconstruction procedure with an analysis window of 10 MeV in the di-pion invariant mass, in $\delta = 5$ case. In graph b) we show the corresponding values of R^2 which quantify the linearity accuracy. In both a) and b) subfigures we have kept only those reconstructed events which possess $R^2 > 0.8$. In graph c) we depict the second factorial moment of a single reconstructed event (with slope less than one fifth standard deviations away from the histogram average), for the same universality class, analysis window and freeze-out time. In graph d) we present the average second factorial moment for the ensemble of reconstructed events.

analysis, contrary to the ensemble averaged one. However, for the majority of events the procedure is successful, and this allows us to acquire the information which would be hidden in an average analysis.

The time-evolution affects the initial geometry of the critical system in a two-fold way: Firstly, the power law weakens, i.e. most of the exponents ζ are smaller than the critical value $f_2 = 2/3$. Secondly, the linearity demanded in relation (16) is spoiled compared to an ideal fractal case. Both these features are obvious in fig. 8. Note that in order to ensure the power-law behavior we

cut in the final analysis the reconstructed events with $R^2 < 0.8$. These events either correspond to a partially unsuccessful reconstruction, or (which is the usual case) their time evolution has significantly spoiled the initial critical profile. In both cases they are of no interest for the purposes of this work, which focus on the survival of criticality. After their elimination we remain with about three fifths of the initial population.

Although time evolution weakens the power-law strength and spoils its form, one can clearly observe strong signs of the initial criticality. That is, the slope $\zeta \approx 0.42$ of fig. 8d is rather large and linearity is satisfactory. This result is displayed more transparently in subfigure 8a. The peak of $\rho(\zeta)$ at small ζ reveals the complete loss of the initial criticality in the majority of events. However, the structure of $\rho(\zeta)$ and especially its secondary peak is a robust sign that the initial fractal geometry has been survived in a subset of events. Quantitatively, we can calculate the average ζ for those events of fig. 8a that are on the right of the minimum that separates the conventional background from the secondary peak. We find $\langle \zeta \rangle_{>\text{min.}} \approx 0.58$, which is very close to the initial value $2/3$ of the critical index. Thus, evolutionary intermittency, in an event-by-event basis, provides a clear and unambiguous measure of revealing the signs of the survived criticality. Finally, we have confirmed that, although always carrying the information of the initial critical geometry, $\langle \zeta \rangle_{>\text{min.}}$ is sensitive to the value of the isothermal critical exponent δ (which determines the universality class). This behavior enhances the robustness of evolutionary intermittency in the investigation of the QCD critical point, and furthermore it supports its use in order to trace the QCD universality class.

V. SUMMARY AND CONCLUSIONS

In this work we have explored, both in physical and momentum space, the dynamics of the critical isoscalar condensate which is expected to be formed near the QCD critical point. For this purpose we have adapted the σ -model Lagrangian in order to describe correctly the characteristics of the order parameter associated with the critical endpoint of the QCD phase transition [15] and we have developed a scheme to propagate the corresponding σ -configurations in momentum space. The issue is of primary importance in the search for the existence and location of the QCD critical point, in experiments with nuclei. At the phenomenological level these fluctuations are expressed through the fractal mass dimension of the σ -field configurations, determining the properties of the condensate at criticality [7, 11].

In particular, we have considered the geometrical deformation of the transverse momentum

pattern of the critical σ 's as a function of time, in terms of factorial moment analysis. To take into account dynamical effects related with this deformation we have introduced the concept of evolutionary intermittency, quantified by the total distribution of the critical indices ζ . We have calculated them by investigating the transverse momentum factorial moments in an event-by-event basis, assuming that each event is characterized by a different decay time lying in the freeze-out zone. Thus, evolutionary intermittency, describing event-by-event dipion pair correlations in transverse momentum space, is the basic observable in our approach. It incorporates, in terms of fractal mass dimension values, all the out-of-equilibrium dynamical history of the critical system. In this context, the main result of our treatment is the survival of critical fluctuations in momentum space even if dynamical effects prevail in the freeze-out era. This survival is expressed as a secondary peak in the distribution of the critical indices representing the evolutionary intermittency profile of the considered process.

The description of the critical fluctuations for the isoscalar condensate within the presented approach is compatible, at least in an approximate scheme, with (a) the sigma dynamics, (b) the initial conditions of a second-order phase transition, (c) the effects in medium and in particular the partial restoration of chiral symmetry and (d) the requirements of observability in nuclear collisions. However, we do not pretend to present a complete picture since the introduced quench scenario does not allow for the parametrization of the freeze-out state of the formed critical condensate in terms of chemical potential and temperature, which are measurable quantities in a heavy-ion collision experiment. In addition we have neglected collective transverse flow phenomena. To incorporate these issues, one should include additional constraints in the dynamics which are beyond the present study. Last but not least, the assumption of pions originating exclusively from critical sigmas and not suffering final-state interactions, constitutes an idealized scenario for the evolution of the critical system. Nevertheless, despite its limitations, the treatment of the present work is a realistic step towards the determination of suitable observables associated with the critical fluctuations in a heavy-ion collision experiment. The obtained results are of interest especially in front of the forthcoming experiments at RHIC and SPS which are expected to reach this region in the QCD phase diagram.

Acknowledgements: The authors acknowledge partial financial support through the research programs “Pythagoras” of the EPEAEK II (European Union and the Greek Ministry of

Education) and “Kapodistrias” of the University of Athens.

-
- [1] Proceedings, RIKEN BNL Research Center Workshop, Vol. **80**, BNL-75692-2006.
- [2] N. G. Antoniou *et al*, Letter of Intent, CERN-SPSC-2006-001.
- [3] F. Karsch, [arXiv:hep-lat/0601013];
 Z. Fodor and S. Katz, JHEP **0404**, 050 (2004) [arXiv:hep-lat/0402006];
 R. V. Gavai and S. Gupta, Phys. Rev. D **71**, 114014 (2005) [arXiv:hep-lat/0412035].
- [4] N. G. Antoniou and A. S. Kapoyannis, Phys. Lett. B **563**, 165 (2003) [arXiv:hep-ph/0211392];
 N. G. Antoniou, F. K. Diakonou and A. S. Kapoyannis, Nucl. Phys. A **759**, 417 (2005) [arXiv:hep-ph/0503176].
- [5] A. Lesne, *Renormalization Methods; Critical Phenomena; Chaos; Fractal Structures*, John Wiley & Sons Ltd, (1998);
 P. M. Chaikin, T. C. Lubensky *Principles of condensed matter physics*, Cambridge University Press (1997).
- [6] N. G. Antoniou, Y. F. Contoyiannis, F. K. Diakonou and G. Mavromanolakis, Nucl. Phys. A **761**, 149 (2005) [arXiv:hep-ph/0505185].
- [7] N. G. Antoniou, Y. F. Contoyiannis, F. K. Diakonou, A. I. Karanikas and C. N. Ktorides, Nucl. Phys. A **693**, 799 (2001) [arXiv:hep-ph/0012164].
- [8] K. Rajagopal and F. Wilczek, [arXiv:hep-ph/0011333].
- [9] J. Berges and K. Rajagopal, Nucl. Phys. B **538**, 215 (1999) [arXiv:hep-ph/9804233];
 M. A. Stephanov, Prog. Theor. Phys. Suppl. **153**, 139 (2004) [arXiv:hep-ph/0402115].
- [10] Y. Hatta and T. Ikeda, Phys. Rev. D **67**, 014028 (2003) [arXiv:hep-ph/0210284];
 N. G. Antoniou, F. K. Diakonou, A. S. Kapoyannis and K. S. Kousouris, Phys. Rev. Lett. **97**, 032002 (2006) [arXiv:hep-ph/0602051].
- [11] N. G. Antoniou, F. K. Diakonou and E. N. Saridakis, Nucl. Phys. A **784**, 536 (2007) [arXiv:hep-ph/0610382].
- [12] A. Bialas and R. Peschanski, Nucl. Phys. B **273**, 703 (1986);
 A. Bialas and R. Peschanski, Nucl. Phys. B **308**, 857 (1988).
- [13] E. A. De Wolf, I. M. Dremin and W. Kittel, Phys. Rept. **270**, 1 (1996) [arXiv:hep-ph/9508325].
- [14] M. Gell-Mann and M. Levy, Nuovo Cim. **16** (1960) 705.
- [15] K. Rajagopal and F. Wilczek, Nucl. Phys. B **399** (1993) 395 [arXiv:hep-ph/9210253].
- [16] S. Gavin, A. Gocksch and R. D. Pisarski, Phys. Rev. Lett. **72**, 2143 (1994) [arXiv:hep-ph/9310228].
- [17] G. Karra, R. J. Rivers, Phys. Lett. B **414**, 28-33 (1997) [arXiv:hep-ph/9705243].
- [18] M. Stephanov, K. Rajagopal and E. Shuryak, Phys. Rev. **D60**, 114028 (1999) [hep-ph/9903292].
- [19] N. G. Antoniou, F. K. Diakonou, E. N. Saridakis, G. A. Tsolias, Physica A **376**, 308 (2007)

- [arXiv:physics/0607038].
- [20] M. M. Tsypin, Phys. Rev. Lett. **73**, 2015 (1994);
J. Berges, N. Tetradis, C. Wetterich, Phys. Rep. **363**, 223 (2002) [arXiv:hep-ph/0005122].
- [21] N. G. Antoniou, Y. F. Contoyiannis, F. K. Diakonov and C. G. Papadopoulos, Phys. Rev. Lett. **81**, 4289 (1998) [arXiv:hep-ph/9810383];
N. G. Antoniou, Y. F. Contoyiannis, F. K. Diakonov, Phys. Rev. E **62**, 3125 (2000) [arXiv:hep-ph/0008047].
- [22] B. B. Mandelbrot, *The Fractal Geometry of Nature*, W. H. Freeman and Company, New York (1983).
- [23] K. Falconer, *Fractal Geometry: Mathematical Foundations and Applications*, John Wiley & Sons, West Sussex (2003).
- [24] R. P. Feynman, talk presented at Argonne Symposium on High Energy Interactions and Multiparticle Production, 1970 (unpublished);
K. Wilson, Cornell Report No. CLNS-131, 1970 [reprinted in *Phenomenology of Particles at High Energies*, proceedings of the Fourteenth Scottish Universities Summer School in Physics, 1973, edited by R. L. Crawford and R. Jennings (Academic, London, 1974)].
- [25] K. B. Blagoev, F. Cooper, J. F. Dawson and B. Mihaila, Phys. Rev. D **64**, 125003 (2001) [arXiv:hep-ph/0106195].
- [26] N. G. Antoniou, F. K. Diakonov, E. N. Saridakis and G. A. Tsolias, Phys. Rev. E **75**, 041111 (2007) [arXiv:physics/0610111].
- [27] T. Hatsuda, T. Kunihiro and H. Shimizu, Phys. Rev. Lett. **82**, 2840 (1999);
T. Hatsuda and T. Kunihiro, Phys. Rep. **247**, 221 (1994);
S. Chiku and T. Hatsuda, Phys. Rev. **D58**, 076001 (1998).